Efficient Light Trapping Structures for Organic Photovoltaics Fabricated by Nanoimprint Lithography

Shigeru Kubota[1*], Kenta Hiraga[1], Kensaku Kanomata[1], Bashir Ahmmad[1], Jun Mizuno[2], and Fumihiko Hirose[1]

[1] *Graduate School of Science and Engineering, Yamagata University,*
4-3-16 Jonan, Yonezawa, Yamagata 992-8510, Japan
[2] *Research Organization for Nano and Life Innovation, Waseda University,*
513 Wasedatsurumaki-cho, Shinjyuku-ku, Tokyo 162-0041, Japan
*kubota@yz.yamagata-u.ac.jp

To improve the efficiency of organic photovoltaics (OPVs), the trapping of incident light with surface nanostructures, such as moth eye structures, is a highly useful strategy for enhancing absorption in the photoactive layer. Nanoimprint lithography is a widely used technique to produce large-area nanostructures cost effectively. However, the moth eye texture fabricated by the nanoimprint process necessarily contains a spatial clearance between adjacent cones, which could degrade the antireflective property of the textured surface. In this study, we perform optical simulations for the OPVs with moth eye coating to explore the effects of the spatial clearance in the moth eye array as well as its geometric pattern on the photocurrent generation. We show that the photocurrent level decreases significantly and superlinearly with increases in the size of the spatial clearance in moth eye, suggesting the importance of sufficiently narrowing the clearance size. Furthermore, we experimentally measure the performance of the OPV cell incorporated with the moth eye structure having a near-optimal geometric pattern with reduced clearance size to verify the simulation results.

Keywords: Organic solar cell, Light trapping, Nanoimprint lithography, FDTD

1. Introduction

Organic photovoltaics (OPVs) are highly promising as cost-effective, large-area, and flexible renewable energy source for the next generation [1, 2]. In addition, OPVs are expected as indoor photovoltaic devices, since the absorption wavelength matches with the indoor light spectrum and the fill factor is relatively high at low light intensities [3-5]. The performance of bulk heterojunction OPV devices has been steadily improving with the development of organic semiconductor materials having lower band gap energy [6,7]. To date, the power conversion efficiency (PCE) of OPVs has attained more than 10% [8], although further improvement would be required for widespread applications.

A challenging factor for further increasing the efficiency of OPVs is to overcome the low level of light absorption in the photoactive layer, which results in substantial current loss [9]. Because organic semiconductors are characterized by low carrier mobility and short exciton diffusion length, the thickness of the active layer is normally limited to 100-200 nm for decreasing recombination loss and facilitating charge extraction [10,11]. However, the use of such thin active layer necessarily causes insufficient absorption of incident photon, resulting in lower carrier generation. Therefore, it would be important to develop antireflection techniques which can efficiently trap light in the thin active layer and allows for maximally utilizing the available photon energy.

The optical manipulation with surface nanostructures, such as moth eye textures, has become an increasingly popular technique for light trapping [11-14]. In the moth eye texturing, which is a structure inspired by the corneal surface of moth's eyes, the device surface is covered with a

periodic array of cones with a period and height of several hundred nanometers. The moth eye surface has the optical property that the effective refractive index changes gradually, which can significantly suppress reflection occurring due to a discontinuous change in the index value [1515,16]. It has been shown by our recent numerical study [17] that the moth eye surface can realize effective light trapping of OPVs by modifying the optical wave propagation and strengthening the electrical field intensity within the active layer. It has been also shown that the photocurrent level of OPVs significantly depends on the precise values of period and height of moth eye texture [17], suggesting that adequately designing the geometric parameters is essential to fully bring out the performance of the nanotexture.

For fabricating the moth eye structure for OPVs, nanoimprint lithography is highly beneficial, because this technique has sufficient compatibility with the advantages of OPVs, such as the low-cost and large-area fabrication [18,19]. In addition, the nanoimprint lithography can be extended to the roll-to-roll manufacturing process, which has the advantages of continuous processing and high throughput adequate for industrial-scale applications [20]. However, in the moth eye structure fabricated by the nanoimprint lithography, it is inevitable that there exists a spatial clearance between adjacent cones [21-24]. This would lead to the degradation of antireflection performance by generating a discontinuous change in the effective refractive index [15].

Therefore, we perform optical simulations for the OPVs incorporated with the moth eye surface with various geometric parameters, and explore the effects of the spatial clearance in the cone array on the performance. In addition, we experimentally fabricate the OPVs with the moth eye having near-optimal geometric characteristics, by using nanoimprint lithography, and test the simulation results.

2. Experimental

2.1. Optical simulation

The simulation based on the finite-difference time-domain (FDTD) method [25] was used to analyze the optical property of the OPV cell with moth eye coating (Fig. 1). The model for the OPV contains the photoactive layer, which is a blend of poly(3-hexylthiophene) (P3HT) and [6,6]-phenyl-C_{61}-butyric acid methyl ester (PCBM), and the hole transporting layer composed of MoO_3 [17,24].
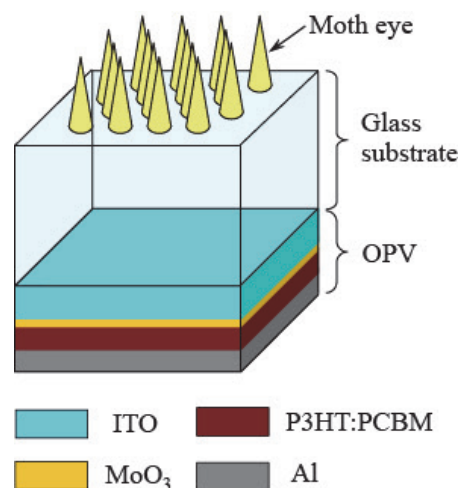

Fig. 1. Device structure of the OPV cell examined in this study.

These layers are sandwiched by the front and back electrodes, which consist of the indium-doped tin oxide (ITO) and Al layers, respectively. Thus, the layer configuration of the OPV is described as ITO (150 nm)/MoO_3 (7 nm)/P3HT:PCBM (100 nm)/Al (100 nm). As shown in Fig. 1, the OPV cell is deposited on the glass substrate whose front surface is coated with moth eye structure. The moth eye is a hexagonal array of cones, and its geometric pattern is characterized by the period L, which is the distance between the tips of adjacent cones, as well as the base diameter D and height H of each cone. The moth eye coating is assumed to be fabricated by using nanoimprint lithography. Therefore, the refractive index of moth eye structure is set as 1.5, which is a typical value for the polymeric resists used in the nanoimprint process [26].

Due to the existence of a glass substrate much thicker than the wavelength, the optical response obtained by the FDTD simulation shows strong wavelength-dependent oscillation, which is not observed in the actual device [17]. To remove such oscillatory component, we applied the envelope method [17,27] to the FDTD response, and accurately estimated the spectrum of the absorbance in the active layer. The absorbance spectrum was converted to the short-circuit current density (J_{SC}) by using the irradiance spectrum of incident light [17,24]. The incident light spectrum is assumed to be AM1.5 standard [28] except for Fig. 3, where the indoor light spectra of LED [29]

and fluorescent lamp [30] are additionally applied. The normal incidence condition is assumed for all the simulations.

2.2. Device fabrication and measurement

The experimentally constructed structure of the OPV cell is the same as that of the model used in the simulation (i.e., ITO/MoO$_3$/P3HT:PCBM/Al). A glass substrate coated by 150-nm ITO (9 Ω/square) was cleaned with acetone, isopropanol, and deionized water in an ultrasonic bath, and subsequently cleaned with UV/ozone. After the 7-nm-thick MoO$_3$ film was evaporated on the surface of ITO, the 100-nm-thick P3HT:PCBM layer was spin coated on the MoO$_3$ layer. Finally, 100-nm-thick Al layer was evaporated on the polymer film, and the device was annealed at 130 ºC for 15 min at nitrogen atmosphere.

To fabricate moth eye nanostructure, a glass substrate was cleaned using organic solvents and UV/ozone, similar to the method mentioned above. A UV curable resin (Toyo Gosei, PAK01) was spin coated onto the glass substrate with 800 nm thickness, and then was annealed at 80 ºC for 2 min. The hexagonal moth eye array (pattern size: 15 mm × 15 mm) was replicated in the resin by the nanoimprint lithography from the mold prepared beforehand, by using the UV nanoimprint device (Engineering System, EUN-4200II). To construct the OPV device with moth eye coating, the glass substrate with OPV was connected with the glass substrate with moth eye by putting between them the contact liquid which has the same refractive index as that of the glass (1.5) [24]. This fabrication method was used for the sake of convenience in comparing the performance of the devices with and without moth eye coating. The current density–voltage (*J–V*) characteristic curve of the OPV cell was measured using a solar simulator (Peccell, PEC-L12) under AM1.5 illumination condition (100 mW/cm^2) at normal incidence.

3. Results and discussion

In the moth eye structure fabricated by nanoimprint lithography, there necessarily exists a spatial gap between adjacent cones, which could decrease the antireflective property [21-24]. We performed FDTD simulations of the OPV cell with moth eye surface (Fig. 1) to examine how the solar cell performance can be modulated by the presence of this processing-dependent factor. To quantify the size of the spatial gap, we define a measure σ =
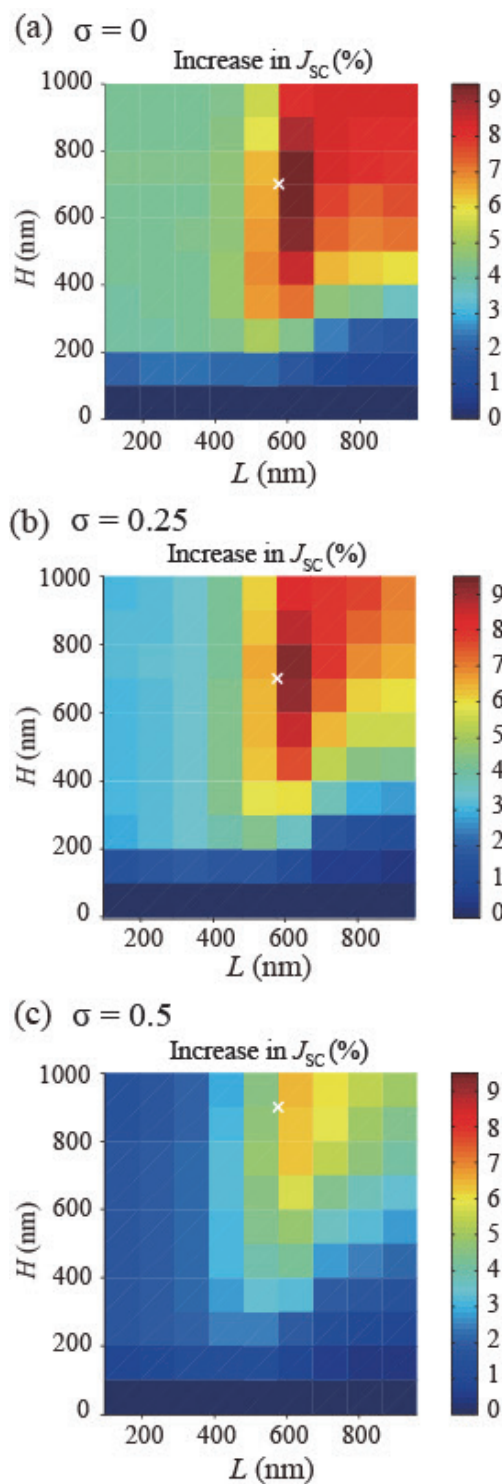

Fig. 2. Effects of the geometric feature of moth eye on the OPV performance. The background color shows the increase rate of J_{SC}, obtained by moth eye coating, as function of the period *L* and height *H* of moth eye. The normalized clearance size in the cone array is σ = 0 (a), 0.25 (b), or 0.5 (c). The x-marks denote the optimal parameters to maximize J_{SC} for each σ (for the detailed parameter values, see Table 1). The discretization step used is 96 nm for *L* and 100 nm for *H*.

Table 1. Optimal values of L and H to maximize J_{SC} and the corresponding increase rate of J_{SC}, predicted by simulation, for each σ.

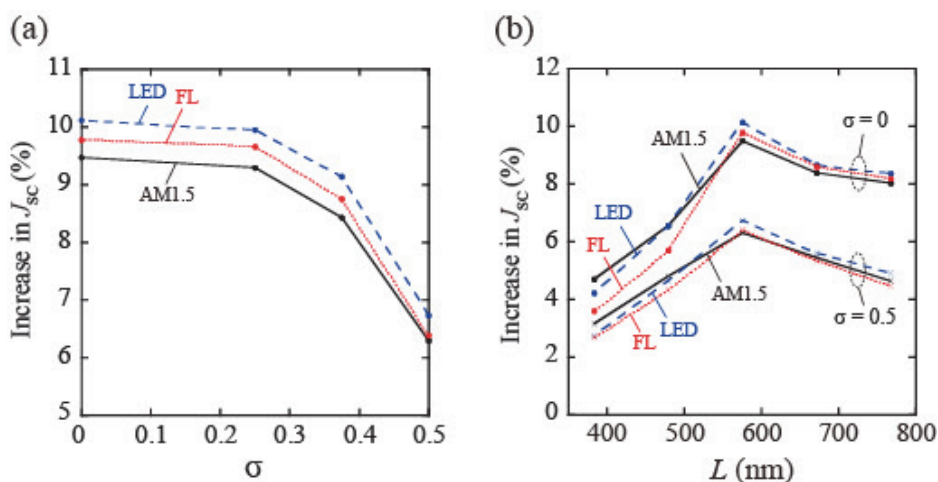| σ	L (nm)	H (nm)	Increase in J_{SC} (%)
0.0	576	700	9.47
0.25	576	700	9.29
0.5	576	900	6.40

Fig. 3. The increase rate of J_{SC}, by introducing moth eye coating, is plotted as function of the normalized clearance size σ (a) or the moth eye period L (b). In (a) and (b), the increase in J_{SC} is calculated using the incident light spectrum of the AM1.5 standard (black), LED (blue), or fluorescent lamp (FL) (red). [Parameter values: (a) L = 576 nm and H = 700 nm (i.e., the optimal parameters for σ = 0 and 0.25 in Table 1). (b) H = 700 nm and σ = 0 or 0.5.]

$(L-D)/L$, with the period L and diameter D of each cone in the moth eye [24]. σ is the length of the clearance between adjacent cones normalized to the texture period, and takes a value between 0 and 1. Figure 2 shows the increase rate of J_{SC} by applying moth eye (as compared to the solar cell without moth eye) as function of L and H, for the three cases of σ (σ = 0, 0.25, and 0.5 in Figs. 2a-2c, respectively). Here, the largest value of σ (= 0.5) is selected because a typical value of σ is 0.4-0.6 for the moth eye fabricated by using the nanoimprint lithography [21-23]. It can be found from Fig. 2 that, for each σ, J_{SC} is significantly increased within a local region around the optimal point (x-marks in the figure) in the parameter space. It is important to note that, as shown in Table 1, the maximum increase rate of J_{SC} for σ = 0.5 (6.40%) is significantly lower than that for σ = 0 and 0.25 (> 9%). This finding is also clarified in Fig. 3a (black line), which expresses the relationship between J_{SC} and σ for L = 576 nm and H = 700 nm (corresponding to the optimal parameter set for smaller σ). The

figure reveals that the increase rate of J_{SC} decreases superlinearly as function of σ so that the degradation of performance becomes particularly severe at larger σ (σ > 0.25). This result indicates that it is quite important to sufficiently decrease the size of the spatial clearance within the moth eye array to fully bring out its performance.

It has been recently suggested that OPVs are also promising as indoor solar cells, because of their relatively high efficiency at low light intensities, as mentioned above [3-5]. Therefore, in Fig. 3, we additionally examined the dependence of J_{SC} on the parameters characterizing the moth eye shape (σ and L in Figs. 3a and 3b, respectively), for the cases of using not only the sunlight [28] but also LED [29] and fluorescent lamp [30] as the incident light spectrum. The results show that the increase level of J_{SC} under the outdoor and indoor light sources are qualitatively similar, and that the superlinear decrease in the increase level of J_{SC}, with increases in σ, can be found independent of the lighting conditions (Fig. 3a). This can be understood from the fact that the
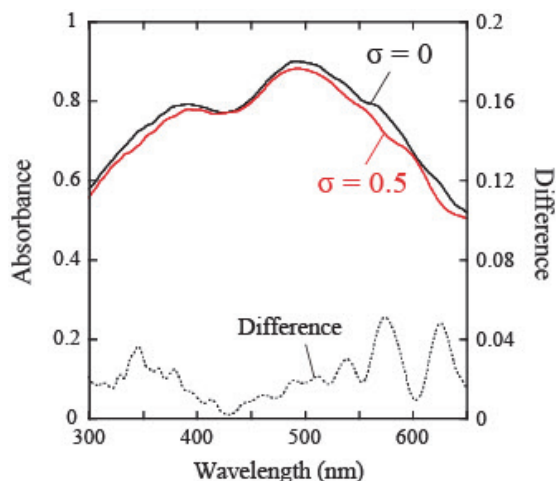
Fig. 4. The solid lines show the spectra of the absorbance in the active layer for $\sigma = 0$ (black) and 0.5 (red) ($L = 576$ nm and $H = 700$ nm). The dotted line is the difference between them.
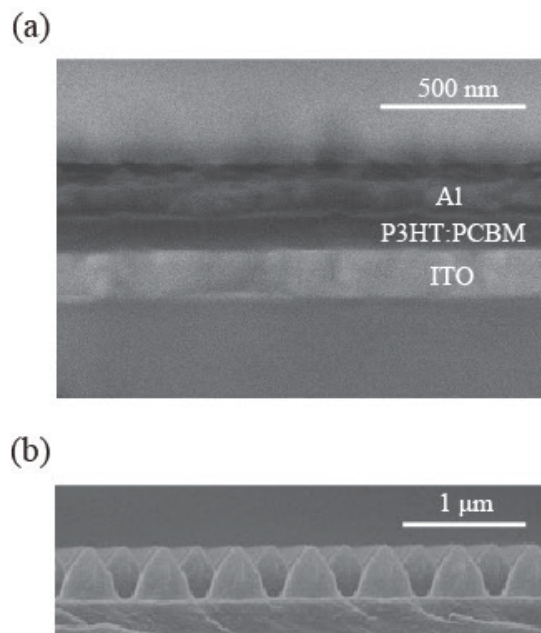

Fig. 5. SEM micrographs of the OPV cell (a) and the moth eye structure produced by nanoimprint lithography (b). In (a), because a slightly oblique cross-section is used, the sample surface can be seen on the upper side of the Al layer. The thin MoO_3 layer (7 nm thickness) is not visible.

spatial gap in the moth eye array causes the decrease in absorption level across a broad wavelength range (Fig. 4), which includes the spectral region where both the outdoor and indoor lights have strong intensity [24].

To verify the prediction by the optical simulation, we experimentally fabricated the moth eye texture, by using nanoimprint lithography, and applied the textured surface to an OPV cell. The layer configuration of the OPV cell as well as the geometric feature of the moth eye were confirmed by SEM observation (Fig. 5). The geometric parameters of the moth eye structure, estimated from the SEM micrograph (Fig. 5b), were as follows: 611 nm period, 467 nm diameter, and 450 nm height (corresponding to the parameters of L, D, and H for the simulation model, respectively). Accordingly, the normalized length of the spatial gap between adjacent moth eye cones was $\sigma = 0.24$. Note that these values of L and H are within the local parameter region around the optimal parameter set in which the performance is quite high, for the case of smaller σ (Figs. 2a and 2b). In addition, the value of σ obtained is small enough to suppress the degradation of performance due to the spatial clearance in the moth eye array (Fig. 3a). Therefore, the moth eye structure used in our experiment can be considered to have near-optimal geometric features predicted by the simulation. The measurement of J-V curves showed a significant increase in J_{SC} by applying the moth eye coating (Fig. 6). As shown in Table 2, the value of J_{SC} increased from 8.84 mA/cm^2 to 9.61 mA/cm^2, corresponding to an increase rate of
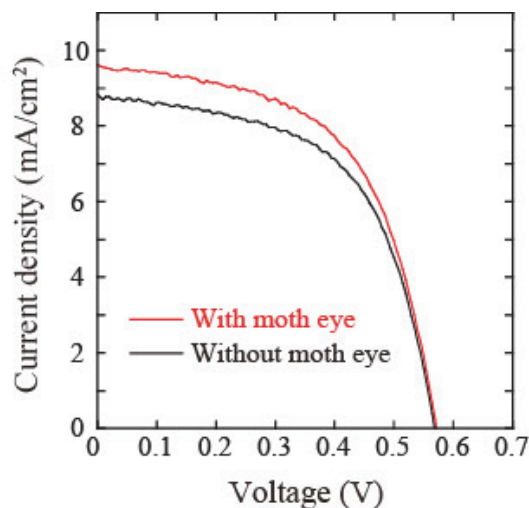

Fig. 6. Current density versus voltage (J-V) characteristic curves of the OPV cell obtained by the experiment. The red and black lines show the cases with and without moth eye coating, respectively.

8.7%. The level of PCE also increased from 2.86% to 3.11%. This change in the efficiency corresponds to a relative increase of 8.7%, which is the same as that of J_{SC}. In contrast, there were not significant changes in the open-circuit voltage (V_{OC}) and fill factor (FF). The relative increase rate

Table 2. The change in the characteristics of the OPV cell by applying moth eye coating (obtained from the *J-V* curves in Fig. 6).

	J_{SC} (mA/cm^2)	V_{OC} (V)	FF	PCE (%)
Without moth eye	8.84	0.565	0.572	2.86
With moth eye	9.61	0.570	0.568	3.11

of J_{SC}, obtained from 7 samples, was summarized as 8.29 ± 0.31% (mean ± s.d.). This increase rate of J_{SC} is slightly below but still comparable to the value predicted by the optical simulation for the case of using the moth eye with the optimal parameters for smaller σ (9.29-9.47%; Table 1).

The experimental result here is in accordance with the simulation result that narrowing the spatial gap in the moth eye array serves to produce higher performance. However, in cases where the OPV cell is used for indoor applications [3-5], it would be highly required that the light trapping function is achieved at not only normal but also oblique incidence. The gradient refractive index profile given by moth eye texturing has been suggested to play a role in weakening reflection at large incident angles by generating smooth optical path of incident light [16]. Thus, it would be an important and promising development direction to explore wide-angle light trapping performance using the nanotextured surface, by extending the current work. Additionally, it would be another important development direction to develop the antireflection nanostructure adequate for the solar cells that utilize the recently developed organic semiconductor materials with wider absorption spectrum [7,31]. Considering that the light trapping effect of moth eye texturing tends to be significantly increased at the wavelength range around the texture period [17], it can be expected that the geometric pattern of nanotexture needs to be adequately designed depending on the wavelength dependent absorption property of the materials.

4. Conclusion

In this study, we have examined both numerically and experimentally the effects of the geometric feature of moth eye surface on its optical property for application to OPVs. It has been clarified that the performance of OPVs significantly depends on the period and height of moth eye array and, furthermore, that higher performance requires a sufficiently narrow spatial clearance between adjacent cones. These results contribute to offering practical design and fabrication methods of surface nanotexture to achieve efficient light trapping of OPVs.

References

1. G. Yu, J. Gao, J. C. Hemmelen, F. Wudl, and A. J. Heeger, *Science*, **270** (1995) 1789.
2. S. H. Park, A. Roy, S. Beaupre, S. Cho, N. Coates, J. S. Moon, D. Moses, M. Leclerc, K. Lee, and A. J. Heeger, *Nat. Photonics*, **3** (2009) 297.
3. B. Minnaert and P. Veelaert, *Proc. SPIE*, **7722** (2010) 77221P.
4. R. Steim, T. Ameri, P. Schilinsky, C. Waldauf, G. Dennler, M. Scharber, and C. J. Brabec, *Sol. Energ. Mater. Sol. Cells*, **95** (2011) 3256.
5. J. Bachmann, C. Buerhop-Lutz, R. Steim, P. Schilinsky, J. A. Hauch, E. Zeira, and B. Christoh, *Sol. Energ. Mat. Sol. Cells*, **101** (2012) 176.
6. Y.-G. Bi, J. Feng, J.-H. Ji, F.-S. Yi, Y.-F. Li, Y.-F. Liu, X.-L. Zhang, and H.-B. Sun, *Nanophotonics*, **7** (2018) 371.
7. Y. Yan, F. Cai, L. Yang, J. Li, Y. Zhang, F. Qin, C. Xiong, Y. Zhou, D. G. Lidzey, and T. Wang, *Adv. Mater.*, **29** (2017) 1604044.
8. M. A. Green, Y. Hishikawa, E. D. Dunlop, D. H. Levi, J. Hohl-Ebinger, M. Yoshita, and A. W. Y. Ho-Baillie, *Prog. Photovolt. Res. Appl.*, **27** (2019) 3.
9. A. Polman, M. Knight, E. C. Garnett, B. Ehrler, and W. C. Sinke, *Science*, **352** (2016) aad4424.
10. Y. Park, K. Vandewal, and K. Leo, *Small Methods*, **2** (2018) 1800123.
11. Q-D. Ou, Y-Q. Li, and J-X. Tang, *Adv. Sci*, **3** (2016) 1600123.
12. R. Brunner, O. Sandfuchs, C. Pacholski, C. Morhard, and J. Spatz, *Laser Photonics Rev.*, **6** (2012) 641.
13. Y. F. Huang and S. Chattopadhyay, *J.*

Nanophotonics, **7** (2013) 073594.

14. S. Kubota, K. Kanomata, T. Suzuki, B. Ahmmad, and F. Hirose, *J. Coat. Technol. Res.*, **12** (2015) 37.

15. A. Deinega, I. Valuev, B. Potapkin, and Y. Lozovik, *J. Opt. Soc. Am. A*, **28** (2011) 770.

16. M. Chen, H. C. Chang, A. S. P. Chang, S. Y. Lin, J. Q. Xi, and E. F. Schubert, *Appl. Opt.*, **46** (2007) 6533.

17. S. Kubota, K. Kanomata, B. Ahmmad, J. Mizuno, and F. Hirose, *J. Coat. Technol. Res.*, **13** (2016) 201.

18. J. John, Y. Y. Tang, J. P. Rothstein, J. J. Watkins, and K. R. Carter, *Nanotechnology*, **24** (2013) 505307.

19. A. Boltasseva, *J. Opt. A.*, **11** (2009) 114001.

20. N. Kooy, K. Mohamed, L. T. Pin, and O. S. Guan, *Nanoscale Res. Lett.*, **9** (2014) 320.

21. L. Zhou, Q.-D. Ou, J.-D. Chen, S. Shen, J.-X. Tang, Y.-Q. Li, and S.-T. Lee, *Sci. Rep.*, **4** (2014) 4040.

22. S.-Y. Chuang, C.-C. Yu, H.-L. Chen, W.-F. Su, and C.-W. Chen, *Sol. Energ. Mater. Sol. Cells*, **95** (2011) 2141.

23. J. Tommila, V. Polojärvi, A. Aho, A. Tukiainen, J. Viheriälä, J. Salmi, A. Schramm, J. M. Kontio, A. Turtiainen, T. Niemi, and M. Guina, *Sol. Energ. Mater. Sol. Cells*, **94** (2010) 1845.

24. S. Kubota, Y. Harada, T. Sudo, K. Kanamata, B. Ahmmad, J. Mizuno, and F. Hirose, *J. Coat. Technol. Res.*, **14** (2017) 1209.

25. A. Taflove and S. C. Hagness, "Computational electrodynamics: The finite-difference time-domain method", Artech House Inc., Norwood (2005).

26. C. Lü and B. Yang, *J. Mater. Chem.*, **19** (2009) 2884.

27. S. Kubota, K. Kanomata, B. Ahmmad, J. Mizuno, and F. Hirose, *J. Photopolym. Sci. Technol.*, **29** (2016) 209.

28. ASTMG173-03, "Standard tables for reference solar spectral irradiances, ASTM International." West Conshohocken, Pennsylvania (2005).

29. B. Minnaert and P. Veelaert, *Energies*, **7** (2014) 1500.

30. Colorimetry, 3rd ed., CIE 15:2004, International Commission on Illumination, Vienna, Austria, 2004.

31. C. Liu, C. Yi, K. Wang, Y. Yang, R. S. Bhatta, M. Tsige, S. Xiao, and X. Gong, *ACS Appl. Mater. Interfaces*, **7** (2015) 4928.